Optical trapping of ultracold dysprosium atoms: transition probabilities, dynamic dipole polarizabilities and van der Waals C_6 coefficients

H Li, Jean-François Wyart, Olivier Dulieu, Maxence Lepers, Sylvain Nascimbène

Optical trapping of ultracold dysprosium atoms: transition probabilities, dynamic dipole polarizabilities and van der Waals C_6 coefficients

H. Li[1], J.-F. Wyart[1,2], O. Dulieu[1], S. Nascimbène[3] and M. Lepers[1]

[1]Laboratoire Aimé Cotton, CNRS, Université Paris-Sud, ENS Cachan, Université Paris-Saclay, 91405 Orsay, France
[2]LERMA, Observatoire de Paris-Meudon, PSL Research University, Sorbonne Universités, UPMC Univ. Paris 6, CNRS UMR8112, 92195 Meudon, France
[3]Laboratoire Kastler Brossel, Collège de France, CNRS, ENS-PSL Research University, UPMC-Sorbonne Universités, 11 place Marcelin Berthelot, 75005 Paris

E-mail: maxence.lepers@u-psud.fr

Abstract. The efficiency of optical trapping of ultracold atoms depend on the atomic dynamic dipole polarizability governing the atom-field interaction. In this article, we have calculated the real and imaginary parts of the dynamic dipole polarizability of dysprosium in the ground and first excited level. Due to the high electronic angular momentum of those two states, the polarizabilities possess scalar, vector and tensor contributions that we have computed, on a wide range of trapping wavelengths, using the sum-over-state formula. Using the same formalism, we have also calculated the C_6 coefficients characterizing the van der Waals interaction between two dysprosium atoms in the two lowest levels. We have computed the energies of excited states and the transition probabilities appearing in the sums, using a combination of *ab initio* and least-square-fitting techniques provided by the Cowan codes and extended in our group. Regarding the real part of the polarizability, for field frequencies far from atomic resonances, the vector and tensor contributions are two-order-of-magnitude smaller than the scalar contribution, whereas for the imaginary part, the vector and tensor contributions represent a noticeable fraction of the scalar contribution. Finally, our anisotropic C_6 coefficients are much smaller than those published in the literature.

1. Introduction

In the field of ultracold gases, *i.e.* with temperatures below 1 milli-kelvin, those containing particles carrying a dipole moment, so-called *dipolar gases*, have attracted tremendous interest during the last years, due to their possibility of exploring strongly correlated matter, with the presence of the long-range, anisotropic dipole-dipole interaction [1, 2]. In contrast with the short-range and isotropic van der Waals interaction, often approximated by contact potentials [3], the dipole-dipole interaction drastically modifies the properties of ultracold gases [4, 5, 6, 7, 8, 9, 10, 11, 12, 13, 14, 15].

Dipolar gases are also promising candidate systems for quantum information and quantum simulation [16, 17, 18, 19].

Dipolar gases can contain different kinds of particles, whose properties can be tailored using electromagnetic fields. Firstly, electric dipole moments can be induced with external electric fields, either in highly-excited, so-called Rydberg atoms [20, 21, 22, 23, 24, 25, 26, 27, 28, 29], or in heteronuclear alkali-metal diatomic molecules [30, 31, 32, 33, 34]. Some of them have been recently produced in their lowest rovibrational and even hyperfine level, *i.e.* LiCs [35], KRb [36, 37, 38], RbCs [39, 40], NaK [41] and NaRb [42]. Open-shell polar molecules such as OH [43], SrF [44], YO [45], RbSr [46], which also possess a (weak) magnetic dipole moment, offer even better possibilities of control. Alternatively, ultracold gases of strong magnetic dipoles have also been produced with chromium [47, 48], high-atomic-number (high-Z) lanthanides [49, 50], including dysprosium (Dy) [51, 52, 53], erbium [54, 55, 56], holmium [57] and thulium [58]. The formation of erbium molecules Er_2 have also been reported [59]. Beyond the scope of dipolar gases, the specific structure of optical transitions in lanthanide atoms could be used to efficiently emulate synthetic gauge fields [60], as recently observed in Ref. [61].

Among neutral atoms, dysprosium presents the strongest magnetic dipole moment, equal to 10 Bohr magnetons (μ_B). This is due to the four unpaired f electrons in the ground-level configuration [Xe]$4f^{10}6s^2$. Moreover, the excited electronic configurations which are close in energy to the lowest one [62], result in a rich energy spectrum, which is not yet completely understood [63, 64, 65]. Dysprosium also presents the particularity of having a pair of quasi-degenerate opposite-parity energy levels with the same electronic angular momentum $J = 10$, which were used for precision measurements [66, 67, 68, 69]. Because the ground and first-excited levels of dysprosium belong to the same configuration and the same LS manifold, *i.e.* ^5I, they possess very similar electronic properties, which make them suitable candidates for optical-clock transitions [70, 71]. Finally, along with erbium [72, 73], dysprosium presents several bosonic and fermionic stable isotopes which allowed for the production of Bose-Einstein condensates and degenerate Fermi gases [74, 75, 76].

In this context, it is crucial to deeply understand and control how the atoms are trapped by electromagnetic fields [77]. The efficiency of the trapping process is determined by the atom-field interaction, and the corresponding ac-Stark shift, which depends on the (complex) dynamic dipole polarizability of the atoms. The real part of the polarizability yields the potential energy exerted on the atomic center of mass, while the imaginary part yields the photon-scattering rate due to spontaneous emission. Because the wave functions associated with the unpaired $4f$ electrons are anisotropic, the ac-Stark shift comprises scalar, vector and tensor contributions, and so it depends on the atomic Zeeman sublevel M_J and the polarization of the electromagnetic field [78, 79]. In this respect, the vector and tensor contributions also determine the strength of the Raman coupling between atomic Zeeman sublevels [60]. In literature, there exist a few theoretical values of the real part of the scalar and tensor static

polarizabilities [80, 81, 82, 83], which are in good agreement with experimental values [84, 85]. By contrast the dynamic polarizability measured in a 1064-nm optical trap [74] is significantly smaller than the theoretical one [86].

In this article, we calculate the real and imaginary parts of the dynamic dipole polarizability for the ground and first excited level of dysprosium, on a wide range of frequencies of the trapping field. We give the scalar, vector and tensor contributions to the polarizability, and the useful formulas to deduce the potential energy and photon-scattering rates in the most frequently used field polarizations $\sigma^{\pm}$ and π. We also calculate the various C_6 coefficients characterizing the van der Waals dispersion interaction between two dysprosium atoms. To get all this information, we take advantage of the flexibility of the sum-over-state formula for polarizability, inherent to second-order perturbation theory. This formula is particularly well adapted to high-Z lanthanide atoms, whose spectrum consists of a few strong transitions in a forest of weak transitions [87]. In addition to the polarizability, we also give precious information on the spectroscopy of dysprosium, whose transition energies and transition dipole moments are computed using a combination of *ab initio* and least-square fitting techniques provided by the Cowan codes [87, 88]. Moreover, in order to adjust experimental and theoretical transition probabilities, we employ the systematic technique that we set up in our previous works on Er^+ [89].

The article is outlined as follows. Section 2 presents in details the results of our electronic-structure calculations, including energy levels (subsections 2.1 and 2.2) and transition probabilities (subsection 2.3). Then the results for the dynamic dipole polarizabilities and C_6 coefficients for the two lowest levels are reported in Section 3. Section 4 contains concluding remarks.

2. Energy levels and transition probabilities

Our electronic-structure calculations were carried out with the Racah-Slater method implemented in the Cowan codes [87], and which were described in our previous papers [79, 88, 89, 90]. Briefly they consist of three steps:

(i) Energies and transition probabilities are computed using a Hartree-Fock method including relativistic corrections and combined with configuration interaction (HFR+CI). For each parity and each value of the total electronic angular momentum J, the the Hamiltonian operator is a combination of angular terms, calculated using Racah algebra, and radial integrals, for example Coulombic or spin-orbit integrals. In addition, transition probabilities depend on monoelectronic transition dipole moments (MTDMs) for each pair of configurations.

(ii) The radial integrals are treated as adjustable parameters, in order to fit the theoretical energies to the experimental ones by a least-square procedure.

(iii) Similarly, the MTDMs are treated as adjustable parameters, in order to fit the theoretical transition probabilities to the experimental ones [91, 92].

For neutral dysprosium (Dy I), the experimental energies are published in the NIST database [63], constructed from the critical compilation of Martin *et. al.* [93], and from Ref. [64] which is posterior to the compilation. For even-parity levels, we also use the yet unpublished work [65]. Note that for bosonic isotopes, the nuclear spin is $I = 0$, and there is no hyperfine structure. By contrast, the fermionic isotopes ^{161}Dy and ^{163}Dy possess a nuclear spin $I = 5/2$, but the resulting hyperfine structure is not considered in the article.

2.1. Energy levels of even parity

The ground level of dysprosium is of even parity with the configuration [Xe]$4f^{10}6s^2$, and total electronic angular momentum $J = 8$. (In what follows, we will omit the confiration of the xenon core [Xe].) The orbital $L = 6$ and spin $S = 2$ angular momenta are also good quantum numbers up to 94 %. Table 1 presents a comparison between our theoretical energies and Landé g-factors with their experimental counterparts. All levels can be labeled in the LS coupling scheme. The levels at $E^{\rm exp} = 13170.38$ and 15636.87 cm^{-1}, not present in the NIST database [63], come from the unpublished list of Ref. [65]. In that work, a careful modeling of the even-parity levels including [Xe]$4f^{10}6s^2$, [Xe]$4f^{10}5d6s$ and [Xe]$4f^96s^26p$ configurations establishes that the two ^5F of Table 1 necessarily belong the [Xe]$4f^{10}6s^2$ configuration. The agreement between theory and experiment is very good, except for the Landé factors of the two highest levels, which indicates that the latter are perturbed by excited configurations. The set of least-square fitted parameters used in this calculation is given in the appendix (see Table A1).

2.2. Energy levels of odd parity

In the odd parity, the electronic configurations included in our model are the two lowest ones $4f^{10}6s6p$ and $4f^95d6s^2$ [62], which are connected to the ground-state configuration $4f^{10}6s^2$ by electric dipole (E1) transitions. Therefore, in our model, we neglect the configuration interaction with other odd-parity configurations, especially $4f^95d^26s$, as it results in numerous levels, making the least-square calculation hard to converge. By contrast, the first parametric study of odd-parity levels was performed with configurations with a limited number of LS terms of the $4f^n$ core, including configuration interaction with $4f^95d^26s$; but such a truncation strongly damaged the quality of the Hamiltonian eigenvectors [95]. In the present study, 126 odd-parity levels were fitted to their known experimental counterparts [63, 64], using 20 free energetic parameters, giving a 44-cm^{-1} standard deviation.

A comparison between theoretical and experimental levels is displayed in Table 2, while the fitted parameters are given in Table A2 of the appendix. All energies are given relative to the $4f^{10}6s^2\ ^5I_8$ ground level. Despite the absence of the $4f^95d^26s$ configuration, whose lowest classified levels is at 18472.71 cm^{-1}, the agreement is very

Table 1. Comparison of energies E through the quantity $\Delta E = E^{\rm exp} - E^{\rm th}$ and Landé g-factors g_L of Dy I even-parity levels of the lowest electronic configuration [Xe]$4f^{10}6s^2$. The superscript "exp" stands for experimental values which are taken from [63, 64]. The superscript "th" stands for the theoretical values from the present parametric calculations (see fitted parameters in Table A1). The "2" in the term $^3K2$ is used to distinguish the ^3K terms coming from different parent terms of the $4f^9$ core (and similarly for $^3H4$) [94]. Therefore those two notations do not have the same meaning as the usual spectroscopic labels $^3H_4$ and $^3K_2$. For those two levels, the numbers between parentheses in the last column, give the total percentage of ^3K and ^3H characters respectively.

Term	J	$E^{\rm exp}$ (cm^{-1})	ΔE (cm^{-1})	$g_L^{\rm exp}$	$g_L^{\rm th}$	% leading term
^5I	8	0	-13	1.242	1.243	94
^5I	7	4143.23	13	1.173	1.175	98
^5I	6	7050.61	7	1.072	1.073	96
^5I	5	9211.58	0.4	0.911	0.911	92
^5I	4	10925.25	-9	0.618	0.618	91
^5F	5	13170.38	7	1.358	1.366	84
^5F	4	15636.87	-6	1.34	1.339	93
$^3K2$	8	19019.15	3	1.14	1.107	58 (75)
$^3H4$	6	24062.88	-2	1.217	1.176	41 (85)

satisfactory. On the contrary, a poor agreement, especially on Landé factors, reflects local perturbations by the $4f^9 5d^2 6s$ configuration.

Table 2: Same as Table 1 for Dy I odd-parity levels. The theoretical values $E^{\rm th}$, the Landé g-factors $g_L^{\rm th}$ and the percentage of configurations and LS terms are derived by means of the Cowan code called "RCG" with the parameter set reported in Table A2. In the configuration notations, A stands for $4f^{10}$, B for $4f^9$, ds^2 for $5d6s^2$, sp for $6s6p$. The lower-case letters or Arabic numbers appearing in the seventh column correspond to different possible parent terms [87]. The terms in parentheses are associated with the core configurations A or B.

$E^{\rm exp}$ (cm^{-1})	$E^{\rm th}$ (cm^{-1})	ΔE (cm^{-1})	$g_L^{\rm exp}$	$g_L^{\rm th}$	Leading configuration	% leading LS term
			$J=2$			
28407.01	28407.9	-1	0.06	0.029	$A-sp$	91 $A-sp\,(^5I)^7H$
			$J=3$			
15254.94	15285.5	-31	0.77	0.777	$B-ds^2$	73 $B-ds^2\,(^6H)^7H$
23824.68	23753.0	72	0.68	0.665	$B-ds^2$	61 $B-ds^2\,(^6H)^5H$
24668.59	24642.8	26	1.29	1.227	$B-ds^2$	22 $B-ds^2\,(^6H)^5F$

Table 2: Odd parity levels of Dy I (continued)

$E^{\rm exp}$ ($\rm cm^{-1}$)	$E^{\rm th}$ ($\rm cm^{-1}$)	ΔE ($\rm cm^{-1}$)	$g_L^{\rm exp}$	$g_L^{\rm th}$	Leading configuration	% leading LS term
26607.16	26647.2	-40	0.58	0.464	$A-sp$	55 $A-sp\,(^5I)^7I$
26886.01	26952.9	-67	1.02	1.075	$B-ds^2$	33 $B-ds^2\,(^6F)^5G$
27321.26	27350.0	-29	0.58	0.551	$A-sp$	31 $A-sp\,(^5I)^7H$
27643.57	27617.4	26	1.17	0.726	$B-ds^2$	61 $B-ds^2\,(^6F)^5H$
28694.51	28720.7	-26	0.55	0.551	$A-sp$	27 $A-sp\,(^5I)^5Ha$
			$J=4$			
13952.00	13984.0	-32	1.082	1.072	$B-ds^2$	67 $B-ds^2\,(^6H)^7H$
16069.98	15986.5	83	1.62	1.627	$B-ds^2$	46 $B-ds^2\,(^6F)^7P$
16412.80	16348.1	65	1.51	1.500	$B-ds^2$	32 $B-ds^2\,(^6H)^7F$
20430.11	20423.4	7	1.28	1.262	$B-ds^2$	36 $B-ds^2\,(^6H)^5G$
20474.99	20457.6	17	1.30	1.373	$B-ds^2$	30 $B-ds^2\,(^6H)^7F$
22099.06	22058.3	41	1.059	1.074	$B-ds^2$	36 $B-ds^2\,(^6H)^5H$
22938.03	22925.4	13	1.07	1.063	$B-ds^2$	25 $B-ds^2\,(^6H)^5F$
23686.81	23663.8	23	0.767	0.743	$B-ds^2$	50 $B-ds^2\,(^6H)^5I$
24841.04	24897.4	-56	0.90	0.881	$A-sp$	39 $A-sp\,(^5I)^7H$
25203.92	25272.1	-68	1.242	1.245	$B-ds^2$	32 $B-ds^2\,(^6F)^5G$
25687.20	25726.2	-39	0.94	0.829	$A-sp$	24 $A-sp\,(^5I)^7I$
26440.41	26446.4	-6	1.046	1.040	$B-ds^2$	55 $B-ds^2\,(^6F)^5H$
26662.41	26716.0	-54	0.59	0.491	$A-sp$	66 $A-sp\,(^5I)^7K$
26998.27	27018.3	-20	0.86	0.865	$A-sp$	41 $A-sp\,(^5I)^7H$
27659.02	27609.3	50	1.17	1.171	$B-ds^2$	34 $B-ds^2\,(^6F)^5G$
27751.46	27746.0	5	0.81	0.742	$A-sp$	45 $A-sp\,(^5I)^3H$
28923.05	28966.4	-43	0.78	0.778	$A-sp$	25 $A-sp\,(^5I)^3H$
33324.06	33281.2	43	0.89	0.890	$A-sp$	39 $A-sp\,(^5I)^5Hb$
33952.33	34025.8	-73	1.30	1.318	$B-ds^2$	9 $B-ds^2\,(^4G)^5D4$
34038.46	34007.8	31	1.30	1.305	$A-sp$	22 $A-sp\,(^5F)^3G$
34486.89	34487.9	-1	1.213	1.344	$A-sp$	21 $A-sp\,(^5F)^5Fa$
34720.68	34704.0	17	0.761	0.659	$A-sp$	43 $A-sp\,(^5I)^5Ib$
			$J=5$			
12298.55	12334.8	-36	1.24	1.233	$B-ds^2$	58 $B-ds^2\,(^6H)^7H$
14153.49	14131.0	22	1.42	1.419	$B-ds^2$	51 $B-ds^2\,(^6H)^7F$
16684.73	16664.2	21	1.082	1.067	$B-ds^2$	66 $B-ds^2\,(^6H)^7I$
17502.89	17506.3	-3	1.45	1.426	$B-ds^2$	33 $B-ds^2\,(^6F)^7D$
17804.24	17834.6	-30	1.322	1.320	$B-ds^2$	44 $B-ds^2\,(^6H)^5F$
19480.87	19563.7	-83	1.35	1.334	$B-ds^2$	29 $B-ds^2\,(^6F)^7G$
19813.98	19794.5	19	1.27	1.281	$B-ds^2$	22 $B-ds^2\,(^6H)^5H$
20921.55	20901.2	20	1.30	1.121	$B-ds^2$	32 $B-ds^2\,(^6H)^5H$
22294.88	22296.6	-2	1.02	0.990	$B-ds^2$	35 $B-ds^2\,(^6H)^5I$

Table 2: Odd parity levels of Dy I (continued)

$E^{\rm exp}$ ($\rm cm^{-1}$)	$E^{\rm th}$ ($\rm cm^{-1}$)	ΔE ($\rm cm^{-1}$)	$g_L^{\rm exp}$	$g_L^{\rm th}$	Leading configuration	% leading LS term
20921.55	20901.2	20	1.30	1.121	$B-ds^2$	32 $B-ds^2\,(^6H)^5H$
22294.88	22296.6	-2	1.02	0.990	$B-ds^2$	35 $B-ds^2\,(^6H)^5I$
22524.21	22498.8	25	1.04	1.052	$A-sp$	19 $A-sp\,(^5I)^7H$
23552.65	23553.9	-1	1.07	1.051	$A-sp$	27 $A-sp\,(^5I)^7I$
24634.07	24637.6	-3	1.21	1.214	$B-ds^2$	37 $B-ds^2\,(^6F)^5H$
24881.87	24938.6	-57	0.72	0.753	$B-ds^2$	70 $B-ds^2\,(^6H)^5K$
25082.02	24997.7	84	1.064	0.992	$A-sp$	41 $A-sp\,(^5I)^7H$
25127.52	25152.4	-25	1.04	0.843	$A-sp$	42 $A-sp\,(^5I)^7K$
25912.63	25892.0	20	0.98	0.979	$A-sp$	30 $A-sp\,(^5I)^3H$
26135.21	26106.5	29	1.22	1.214	$B-ds^2$	30 $B-ds^2\,(^6F)^5G$
27109.93	27140.3	-30	1.01	0.993	$A-sp$	23 $A-sp\,(^5I)^7I$
27685.87	27695.2	-9	0.77	0.765	$A-sp$	31 $A-sp\,(^5I)^5Ka$
29054.36	29112.4	-58	0.84	0.871	$A-sp$	32 $A-sp\,(^5I)^3I$
30904.89	30885.3	19	1.286	1.159	$A-sp$	29 $A-sp\,(^5I)^5Hb$
31763.85	31762.6	1	1.32	1.342	$A-sp$	28 $A-sp\,(^5F)^3G$
33025.64	32950.1	75	1.01	0.923	$A-sp$	38 $A-sp\,(^5I)^5Ib$
33652.23	33639.7	13	1.16	1.254	$B-ds^2$	12 $B-ds^2\,(^4G)^5G4$
34470.70	34513.4	-43	0.915	0.715	$A-sp$	48 $A-sp\,(^5I)^5Kb$
			$J=6$			
10088.80	10146.1	-57	1.36	1.357	$B-ds^2$	36 $B-ds^2\,(^6H)^7H$
11673.49	11649.2	24	1.392	1.395	$B-ds^2$	49 $B-ds^2\,(^6H)^7F$
14970.70	15006.3	-36	1.24	1.238	$B-ds^2$	42 $B-ds^2\,(^6H)^7I$
15862.64	15862.7	0	1.257	1.260	$B-ds^2$	51 $B-ds^2\,(^6H)^5G$
16591.38	16522.4	69	1.348	1.356	$B-ds^2$	59 $B-ds^2\,(^6H)^7G$
18172.87	18254.0	-81	1.34	1.305	$B-ds^2$	22 $B-ds^2\,(^6H)^5H$
18561.20	18629.5	-68	1.27	1.301	$B-ds^2$	20 $B-ds^2\,(^6H)^5H$
18711.93	18724.8	-13	1.172	1.171	$A-sp$	42 $A-sp\,(^5I)^3H$
19182.66	19157.5	25	1.036	1.032	$B-ds^2$	63 $B-ds^2\,(^6H)^7K$
19856.88	19862.5	-6	1.35	1.314	$B-ds^2$	38 $B-ds^2\,(^6F)^7H$
20554.73	20531.2	23	1.11	1.107	$B-ds^2$	29 $B-ds^2\,(^6H)^5I$
20817.61	20798.4	19	1.13	1.135	$A-sp$	17 $A-sp\,(^5I)^7I$
22286.87	22281.7	5	1.15	1.151	$A-sp$	38 $A-sp\,(^5I)^7H$
22633.23	22669.9	-36	1.29	1.297	$B-ds^2$	54 $B-ds^2\,(^6F)^5G$
22956.84	22985.1	-28	1.06	1.083	$A-sp$	22 $A-sp\,(^5I)^7K$
23464.02	23492.1	-28	0.96	0.946	$B-ds^2$	67 $B-ds^2\,(^6H)^5K$
23687.87	23640.9	47	1.076	1.064	$A-sp$	16 $A-sp\,(^5I)^7K$
24040.59	24026.1	14	1.26	1.263	$B-ds^2$	31 $B-ds^2\,(^6F)^5H$
24931.63	24936.8	-5	1.128	1.115	$A-sp$	31 $A-sp\,(^5I)^7I$

Table 2: Odd parity levels of Dy I (continued)

$E^{\rm exp}$ ($\rm cm^{-1}$)	$E^{\rm th}$ ($\rm cm^{-1}$)	ΔE ($\rm cm^{-1}$)	$g_L^{\rm exp}$	$g_L^{\rm th}$	Leading configuration	% leading LS term
25825.83	25836.0	-10	1.00	0.995	$A-sp$	29 $A-sp\,(^5I)^7K$
27199.20	27226.9	-27	1.16	1.032	$A-sp$	16 $A-sp\,(^5I)^3K$
28119.93	28065.6	54	1.198	1.193	$A-sp$	46 $A-sp\,(^5I)^5Hb$
29447.11	29428.2	19	0.90	0.898	$A-sp$	56 $A-sp\,(^5I)^3K$
30778.96	30732.5	46	1.17	1.073	$A-sp$	42 $A-sp\,(^5I)^5Ib$
32126.16	32096.3	30	1.23	1.209	$B-ds^2$	16 $B-ds^2\,(^4F)^5G3$
			$J=7$			
8519.21	8595.5	-76	1.336	1.338	$B-ds^2$	59 $B-ds^2\,(^6H)^7H$
12655.13	12695.4	-40	1.36	1.356	$B-ds^2$	61 $B-ds^2\,(^6H)^7G$
14367.81	14291.7	76	1.27	1.269	$B-ds^2$	46 $B-ds^2\,(^6H)^7I$
15194.83	15243.3	-48	1.26	1.263	$B-ds^2$	60 $B-ds^2\,(^6H)^5H$
16693.87	16659.2	34	1.22	1.227	$A-sp$	23 $A-sp\,(^5I)^5Ha$
17687.90	17681.1	6	1.16	1.152	$B-ds^2$	44 $B-ds^2\,(^6H)^7K$
18339.80	18349.3	-10	1.21	1.197	$B-ds^2$	15 $B-ds^2\,(^6H)^7K$
18433.76	18429.4	4	1.20	1.195	$A-sp$	23 $A-sp\,(^5I)^3I$
18857.04	18807.7	49	1.335	1.323	$B-ds^2$	35 $B-ds^2\,(^6F)^7H$
19907.51	19904.9	3	1.23	1.237	$A-sp$	26 $A-sp\,(^5I)^7I$
20485.40	20501.7	-16	1.375	1.381	$B-ds^2$	64 $B-ds^2\,(^6F)^7G$
20766.29	20720.7	46	1.16	1.140	$A-sp$	19 $A-sp\,(^5I)^5Ka$
21675.28	21698.5	-23	1.22	1.265	$B-ds^2$	41 $B-ds^2\,(^6F)^5H$
21783.41	21766.6	17	1.15	1.110	$B-ds^2$	58 $B-ds^2\,(^6H)^5K$
22061.29	22052.6	9	1.18	1.184	$A-sp$	28 $A-sp\,(^5I)^7I$
23479.77	23482.0	-2	1.13	1.135	$A-sp$	33 $A-sp\,(^5I)^7K$
24708.97	24772.3	-63	1.26	1.265	$A-sp$	38 $A-sp\,(^5I)^5Hb$
24906.86	24912.5	-6	1.14	1.147	$A-sp$	26 $A-sp\,(^5I)^7I$
27427.08	27410.6	17	1.06	1.067	$A-sp$	28 $A-sp\,(^5I)^3K$
27834.93	27850.4	-16	1.22	1.169	$A-sp$	47 $A-sp\,(^5I)^5Ib$
30711.72	30760.7	-49	1.09	1.068	$A-sp$	46 $A-sp\,(^5I)^5Kb$
31698.32	31700.2	-2	1.131	1.125	$B-ds^2$	17 $B-ds^2\,(^4I)^5I3$
			$J=8$			
7565.61	7586.7	-21	1.352	1.356	$B-ds^2$	77 $B-ds^2\,(^6H)^7H$
12007.12	11949.8	57	1.28	1.278	$B-ds^2$	49 $B-ds^2\,(^6H)^7I$
14625.64	14683.1	-57	1.25	1.252	$B-ds^2$	61 $B-ds^2\,(^6H)^5I$
15567.38	15556.1	11	1.31	1.322	$A-sp$	58 $A-sp\,(^5I)^7H$
16288.73	16220.7	68	1.19	1.187	$B-ds^2$	47 $B-ds^2\,(^6H)^7K$
16733.20	16677.7	55	1.20	1.198	$A-sp$	33 $A-sp\,(^5I)^3K$
18021.89	18025.3	-3	1.23	1.230	$A-sp$	23 $A-sp\,(^5I)^3K$
19092.30	19026.8	65	1.33	1.342	$B-ds^2$	77 $B-ds^2\,(^6F)^7H$

Table 2: Odd parity levels of Dy I (continued)

$E^{\rm exp}$ ($\rm cm^{-1}$)	$E^{\rm th}$ ($\rm cm^{-1}$)	ΔE ($\rm cm^{-1}$)	$g_L^{\rm exp}$	$g_L^{\rm th}$	Leading configuration	% leading LS term
19688.60	19655.1	33	1.22	1.200	$B-ds^2$	47 $B-ds^2\,(^6H)^5K$
20341.32	20331.9	10	1.23	1.230	$A-sp$	30 $A-sp\,(^5I)^7K$
21899.20	21874.7	25	1.20	1.210	$A-sp$	33 $A-sp\,(^5I)^7I$
23877.74	23844.6	33	1.29	1.239	$A-sp$	48 $A-sp\,(^5I)^5Ib$
24999.58	24976.9	23	1.19	1.172	$A-sp$	36 $A-sp\,(^5I)^7K$
27818.00	27871.1	-53	1.21	1.154	$A-sp$	45 $A-sp\,(^5I)^5Kb$
			$J=9$			
9990.97	9991.2	0	1.32	1.320	$B-ds^2$	86 $B-ds^2\,(^6H)^7I$
13495.93	13463.1	32	1.23	1.233	$B-ds^2$	60 $B-ds^2\,(^6H)^5K$
15972.35	15972.8	0	1.29	1.294	$A-sp$	61 $A-sp\,(^5I)^7I$
16717.79	16749.8	-32	1.24	1.242	$B-ds^2$	62 $B-ds^2\,(^6H)^7K$
17727.15	17699.8	27	1.25	1.258	$A-sp$	31 $A-sp\,(^5I)^7I$
21838.55	21798.5	40	1.25	1.244	$A-sp$	64 $A-sp\,(^5I)^7K$
23736.61	23788.7	-52	1.22	1.217	$A-sp$	48 $A-sp\,(^5I)^5Ka$
			$J=10$			
12892.76	12992.5	-99	1.29	1.294	$B-ds^2$	94 $B-ds^2\,(^6H)^7K$
17513.33	17465.2	48	1.30	1.295	$A-sp$	94 $A-sp\,(^5I)^7K$

2.3. Transition probabilities

Since they depend on transition dipole moments, the transition probabilities turn out to be an efficient test for the quality of our computed eigenvectors. After the last CI calculation by the Cowan code called "RCG", the eigenvector of the level i can be written $|i\rangle = \sum_p c_{ip}|p\rangle$, where $|p\rangle$ represents an electronic configuration. Then the theoretical Einstein coefficients $A_{ij}^{\rm th}$ characterizing the probability of spontaneous emission from level i to level j can be expanded

$$A_{ij}^{\rm th} = \left(\sum_{pq} a_{ij,pq} \left\langle n\ell, p \right| \hat{r} \left| n'\ell', q \right\rangle \right)^2 , \tag{1}$$

in which the MTDMs $\left\langle n\ell, p \right| \hat{r} \left| n'\ell', q \right\rangle$ are common parameters to all transitions, and the coefficients $a_{ij,pq}$ depend on the energies and eigenvectors characterizing the levels i and j. The configurations included in our model give rise to two possible $\hat{r}$-matrix elements: one for ($n\ell$-$n'\ell'$) = (6s-6p) transitions, namely $(p,q) = (4f^{10}6s^2, 4f^{10}6s6p)$, and the other one for ($n\ell$-$n'\ell'$) = (4f-5d) transitions, namely $(p,q) = (4f^{10}6s^2, 4f^9 5d6s^2)$.

Similarly to section 2.2, our theoretical A coefficients depend on a restricted number of scaling factors (SFs) f_m, which are also adjusted by fitting to available experimental data [96]. The f_m can be defined from MTDMs and their computed HFR values, $f_m = \left\langle n\ell, p \right| \hat{r} \left| n'\ell', q \right\rangle / \left\langle n\ell, p \right| \hat{r} \left| n'\ell', q \right\rangle_{\rm HFR}$. We specify f_1 and f_2 for (6s-6p) and (4f-5d) transitions respectively. From Ref. [96], we can get 80 transitions towards the ground

level $^5I_8$ and first excited one $^5I_7$. As energy increases, especially above 30000 cm^{-1}, it is hard to describe accurately the energy levels only with the $4f^{10}6s6p$ and $4f^95d6s^2$ configurations (see Table 2). Therefore we exclude from the fitting procedure these transitions with upper levels above 30000 cm^{-1}.

Table 3: Transitions excluded from the least-square fitting procedure. The letters i and j correspond to upper and lower levels, respectively. The superscript "exp" stands for experimental values which are taken from [96]. The superscript "th" stands for the theoretical values from the present parametric calculations. The transition wave number σ_{ij} is in the vacuum. The notation (n) stands for $\times 10^n$. A blank in the column "removal reason" means that the upper level belongs neither to the $4f^{10}6s6p$ nor to the $4f^95d6s^2$ configuration.

$E_i^{\rm exp}$ (cm^{-1})	J_i	$E_j^{\rm exp}$ (cm^{-1})	J_j	$\sigma_{ij}^{\rm exp}$ (cm^{-1})	$A_{ij}^{\rm exp}$ (s^{-1})	removal reason
29119	9	0	8	29119	2.32(6)	
27851	8	0	8	27851	3.26(5)	
27556	7	0	8	27556	1.75(5)	
27014	9	0	8	27014	1.19(8)	spurious?
25012	8	0	8	25012	0.37(6)	
24906	7	0	8	24906	2.93(6)	large ratio
24229	9	0	8	24229	0.92(6)	
24204	8	0	8	24204	1.76(6)	
23832	8	0	8	23832	8.80(7)	mixed[a]
20766	7	0	8	20766	0.28(5)	small ratio
20341	8	0	8	20341	1.06(5)	small ratio
28823	7	4134	7	24688	2.54(6)	
28030	8	4134	7	23895	8.80(7)	
27984	7	4134	7	23850	7.10(7)	mixed[b]
27851	8	4134	7	23717	8.10(7)	mixed[c]
27556	7	4134	7	23422	1.14(6)	
25012	8	4134	7	20878	1.08(5)	
18022	8	4134	7	13888	0.65(4)	small ratio
15195	7	4134	7	11061	0.43(5)	small ratio

[a] mixed with level at 23878 cm^{-1}; [b] with level at 27834 cm^{-1}; [c] with level at 27818 cm^{-1}.

In the list of Ref. [96], we can see some strong transitions whose upper level does not belong to $4f^{10}6s6p$ or $4f^95d6s^2$ configurations, *e.g.* $E^{exp} = 23832.060$ cm^{-1}, $J = 8$, but is very close in energy to a $4f^{10}6s6p$ level with the same J, *e.g.* $E^{exp} = 23877.739$ cm^{-1}. This suggests that the former level possess a significant $4f^{10}6s6p$ character in addition to the $4f^95d^26s$ one. However in our model, we can only describe one level,

denoted $|4f^{10}6s6p\rangle \equiv |1\rangle$, which can explain the poor agreement on its Landé factor (see Table 2). Assuming that the two "real", mixed levels, denoted $|+\rangle$ and $|-\rangle$, are isolated from the others, we can write

$$\begin{aligned} |+\rangle &= c_1|4f^{10}6s6p\rangle + c_2|4f^9 5d^2 6s\rangle \\ |-\rangle &= -c_2|4f^{10}6s6p\rangle + c_1|4f^9 5d^2 6s\rangle \end{aligned} \quad (2)$$

with $|c_1|^2 + |c_2|^2 = 1$. We recall that the transition probability depends on the transition frequency ω_{ij} and the reduced transition dipole moment $\langle i\|\hat{d}\|j\rangle$, as $A_{ij} \propto \omega_{ij}^3 |\langle i\|\hat{\mathbf{d}}\|j\rangle|^2$. In our case ($i = 1$, $+$ or $-$), the transition frequencies are equal, $\omega_{1,j} \approx \omega_{+,j} \approx \omega_{-,j}$, whereas the transition dipole moments are such that $|\langle 1\|\hat{\mathbf{d}}\|j\rangle|^2 = |\langle +\|\hat{\mathbf{d}}\|j\rangle|^2 + |\langle -\|\hat{\mathbf{d}}\|j\rangle|^2$. Therefore we compare our theoretical value $A_{1,j}^{\rm th}$ with the sum of experimental ones $A_{+,j}^{\rm exp} + A_{-,j}^{\rm exp}$. In Table 3, the 3 transitions labeled "mixed" correspond to that situation.

Special attention should be paid to the transition between the ground level and the excited $J = 9$ level at 27014.02 cm^{-1}. By comparison with neighboring elements like holmium, the existence of this very strong transition, in addition to the "usual" one with upper level $4f^{10}(^5I_8)6s6p(^1P_1^o)\,(8,1)_9^o$ at 23736.610 cm^{-1}, is all the more questionable, that the level at 27014.02 cm^{-1} does not appear in any other transition. It is probable that this transition exists, *i.e.* its transition energy and transition probability are correct; but its lower level is probably not the ground one, and the upper level $J = 9$ level at 27014.02 cm^{-1} does not exist. Finally, due to strong differences between $A_{ij}^{\rm th}$ and $A_{ij}^{\rm exp}$, we excluded 5 of the last 48 transitions (one with large ratio $A_{ij}^{\rm th}/A_{ij}^{\rm exp}$, while other four with very small ratios).

We fitted the SFs using the remaining 43 transitions, and found optimal scaling factors $f_1 = 0.794$, $f_2 = 0.923$, corresponding to a standard deviation on Einstein coefficients (see Ref. [79], Eq. (15)) $\sigma_A = 2.66 \times 10^6$ s^{-1}. In particular the 6 strongest transitions are calculated with a precision better than 7 %. Then, because the experimental Einstein coefficients in Ref. [96] are given with uncertainties reaching to 10 %, we made 1000 fits in which all the $A_{ij}^{\rm exp}$ coefficients have a random value within their uncertainty range. We obtain optimal scaling factors with statistical uncertainties: $f_1 = 0.794 \pm 0.006$ and $f_2 = 0.923 \pm 0.21$. The standard deviation is therefore much more sensitive to $\langle 6s|\hat{r}|6p\rangle$ than to $\langle 4f|\hat{r}|5d\rangle$, since it involves the strongest transitions [79, 89]. In what follows, we take the optimal scaling factors $f_1 = 0.794$ and $f_2 = 0.923$, for which a comparison between experimental and theoretical transition probabilities involving the two lowest levels of Dy I are presented in Table 4. Using those optimal SFs, we can also calculate transition probabilities which have not been measured, and which are available upon request to the authors.

Table 4: Comparison of Einstein-A coefficients. The superscript "exp" stands for experimental values which are taken from [96]. The superscript "th" stands for the theoretical values from the present calculations. The notation (n) stands for $\times 10^n$. Values with an asterisk $(^*)$ correspond to sums of experimental Einstein coefficients (see Table 3).

$E_i^{\rm exp}$ (cm^{-1})	J_i	$E_j^{\rm exp}$ (cm^{-1})	J_j	$\omega_{ij}^{\rm exp}$ (cm^{-1})	$A_{ij}^{\rm exp}$ (s^{-1})	$A_{ij}^{\rm th}$ (s^{-1})
25000	8	0	8	25000	1.63(5)	2.15(5)
24709	7	0	8	24709	1.92(8)	1.91(8)
23878	8	0	8	23878	2.14(8)*	2.13(8)
23737	9	0	8	23737	2.08(8)	2.09(8)
21899	8	0	8	21899	6.60(5)	1.67(5)
21839	9	0	8	21839	1.96(6)	6.52(5)
21783	7	0	8	21783	1.37(7)	6.64(6)
21675	7	0	8	21675	8.20(6)	1.13(7)
20485	7	0	8	20485	5.20(5)	2.02(5)
19689	8	0	8	19689	4.10(5)	2.97(5)
18857	7	0	8	18857	8.50(5)	4.65(5)
18022	8	0	8	18022	3.00(5)	9.98(4)
17727	9	0	8	17727	4.90(5)	2.78(5)
17688	7	0	8	17688	4.46(5)	1.29(5)
16733	8	0	8	16733	4.20(5)	9.58(5)
16694	7	0	8	16694	5.61(5)	1.32(6)
15972	9	0	8	15972	8.90(5)	1.11(6)
15195	7	0	8	15195	7.70(5)	2.96(5)
28120	6	4134	7	23986	1.92(8)	1.83(8)
27835	7	4134	7	23701	1.91(8)*	2.03(8)
27818	8	4134	7	23684	2.09(8)*	2.06(8)
27427	7	4134	7	23293	2.28(6)	1.77(6)
25000	8	4134	7	20865	1.16(6)	4.53(5)
24907	7	4134	7	20773	2.58(6)	3.89(4)
24709	7	4134	7	20575	2.59(5)	7.50(4)
24041	6	4134	7	19906	1.27(6)	8.12(5)
21899	8	4134	7	17765	1.66(5)	1.12(5)
21783	7	4134	7	17649	3.30(4)	2.57(4)
21675	7	4134	7	17541	1.67(5)	6.21(4)
20766	7	4134	7	16632	5.90(5)	1.10(6)
20555	6	4134	7	16421	1.46(6)	1.14(6)
20485	7	4134	7	16351	5.70(4)	3.66(4)
20341	8	4134	7	16207	8.10(5)	1.14(6)

Table 4: Einstein-A coefficients (continued)

$E_i^{\rm exp}$ (cm^{-1})	J_i	$E_j^{\rm exp}$ (cm^{-1})	J_j	$\sigma_{ij}^{\rm exp}$ (cm^{-1})	$A_{ij}^{\rm exp}$ (s^{-1})	$A_{ij}^{\rm th}$ (s^{-1})
19689	8	4134	7	15554	4.50(4)	1.97(4)
18857	7	4134	7	14723	2.90(4)	1.15(4)
17688	7	4134	7	13554	1.10(5)	1.96(4)
16733	8	4134	7	12599	1.36(4)	5.95(3)

3. Polarizabilities and van der Waals C_6 coefficients

The optimal set of spectroscopic data obtained in the previous section will now be used to compute polarizabilities and van der Waals C_6 coefficients, obtained using the sum-over-state formula inherent to second-order perturbation theory, for the ground level $4f^{10}6s^2\,{}^5I_8$ and the first-excited level $4f^{10}6s^2\,{}^5I_7$ of dysprosium. Indeed the electric-quadrupole transitions between $4f^n6s^2$ levels were suggested as candidates for optical clocks [70, 71], as those levels are expected to possess very similar polarizabilities.

3.1. Polarizabilities

Polarizability is an important characteristic governing the optical trapping of neutral atoms, through their interaction with laser fields. The real part of the (complex) polarizability determines the depth of dipole traps or optical-lattice wells, while the imaginary part determines the photon-scattering rate, which limits the coherence and the trap lifetime for the atoms. The sum-over-state formula enables us to give the real and imaginary parts of the dynamic dipole polarizability at any trapping frequency. Because dysprosium is an open $4f$-shell atom, the trap depths and photon-scattering rate are functions of scalar, vector and tensor polarizabilities, which we give in this article.

3.1.1. Theory of optical trapping. For the sake of consistency, let us recall the useful relationships of optical trapping (see *e.g.* Refs. [77, 78, 79]). We assume that the atoms are in the level $|\beta J M_J\rangle$, where J is the total electronic angular momentum, M_J the azimuthal quantum number associated with its projection on the quantization axis z and β designates all the remaining quantum numbers. We also assume that the atoms are submitted to a laser beam of angular frequency ω and whose intensity $I(\mathbf{r})$ depends on the position $\mathbf{r}$ of the atomic center of mass. If the electric field of the laser beam is linearly polarized along the quantization axis z (π polarization), due to second-order Stark effect, it induces a potential energy $U_{M_J}^{\rm lin}(\mathbf{r})$ acting on the atomic center of mass,

$$U_{M_J}^{\rm lin}(\mathbf{r}) = -\frac{1}{2\epsilon_0 c} I(\mathbf{r}) \left(\Re[\alpha_{\rm scal}(\omega)] + \frac{3M_J^2 - J(J+1)}{J(2J-1)} \Re[\alpha_{\rm tens}(\omega)] \right) \qquad (3)$$

and a photon-scattering rate

$$\Gamma_{M_J}^{\rm lin}(\mathbf{r}) = \frac{1}{\hbar\epsilon_0 c} I(\mathbf{r}) \left(\Im[\alpha_{\rm scal}(\omega)] + \frac{3M_J^2 - J(J+1)}{J(2J-1)} \Im[\alpha_{\rm tens}(\omega)] \right), \qquad (4)$$

which both depend on the atomic Zeeman sublevel M_J. For a right (left) circularly polarized electric field propating along z ($\sigma^{\pm}$ polarization), the potential and photon-scattering rate read

$$U^{\rm circ}_{M_J}(\mathbf{r}) = -\frac{1}{2\epsilon_0 c} I(\mathbf{r}) \left(\Re[\alpha_{\rm scal}(\omega)] \pm \frac{M_J}{2J} \Re[\alpha_{\rm vect}(\omega)] - \frac{3M_J^2 - J(J+1)}{2J(2J-1)} \Re[\alpha_{\rm tens}(\omega)] \right) \tag{5}$$

$$\Gamma^{\rm circ}_{M_J}(\mathbf{r}) = \frac{1}{\hbar\epsilon_0 c} I(\mathbf{r}) \left(\Im[\alpha_{\rm scal}(\omega)] \pm \frac{M_J}{2J} \Im[\alpha_{\rm vect}(\omega)] - \frac{3M_J^2 - J(J+1)}{2J(2J-1)} \Im[\alpha_{\rm tens}(\omega)] \right). \tag{6}$$

In equations (3)–(6), $\Re[]$ and $\Im[]$ stand for the real and imaginary parts of the scalar $\alpha_{\rm scal}$, vector $\alpha_{\rm vect}$ and tensor $\alpha_{\rm tens}$ dynamic dipole polarizabilities given by

$$\alpha_{\rm scal}(\omega) = \frac{1}{3(2J+1)} \sum_{\beta'' J''} |\langle \beta'' J'' \| \mathbf{d} \| \beta J \rangle|^2 \times \left(\frac{1}{E_{\beta'' J''} - E_{\beta J} - i\frac{\hbar\gamma_{\beta'' J''}}{2} - \hbar\omega} + \frac{1}{E_{\beta'' J''} - E_{\beta J} - i\frac{\hbar\gamma_{\beta'' J''}}{2} + \hbar\omega} \right) \tag{7}$$

$$\alpha_{\rm vect}(\omega) = \sqrt{\frac{6J}{(J+1)(2J+1)}} \sum_{\beta'' J''} (-1)^{J+J''} \left\{ \begin{array}{ccc} 1 & 1 & 1 \\ J & J & J'' \end{array} \right\} |\langle \beta'' J'' \| \mathbf{d} \| \beta J \rangle|^2 \times \left(\frac{1}{E_{\beta'' J''} - E_{\beta J} - i\frac{\hbar\gamma_{\beta'' J''}}{2} - \hbar\omega} - \frac{1}{E_{\beta'' J''} - E_{\beta J} - i\frac{\hbar\gamma_{\beta'' J''}}{2} + \hbar\omega} \right) \tag{8}$$

$$\alpha_{\rm tens}(\omega) = 2\sqrt{\frac{5J(2J-1)}{(J+1)(2J+1)(2J+3)}} \sum_{\beta'' J''} (-1)^{J+J''} \left\{ \begin{array}{ccc} 1 & 1 & 2 \\ J & J & J'' \end{array} \right\} |\langle \beta'' J'' \| \mathbf{d} \| \beta J \rangle|^2 \times \left(\frac{1}{E_{\beta'' J''} - E_{\beta J} - i\frac{\hbar\gamma_{\beta'' J''}}{2} - \hbar\omega} + \frac{1}{E_{\beta'' J''} - E_{\beta J} - i\frac{\hbar\gamma_{\beta'' J''}}{2} + \hbar\omega} \right) \tag{9}$$

where $\langle \beta'' J'' \| \mathbf{d} \| \beta J \rangle$ is the reduced matrix element of the transition-dipole-moment operator between the level $|\beta J\rangle$ under consideration and the intermediate level $|\beta'' J''\rangle$, and $\gamma_{\beta'' J''}$ the radiative relaxation rate (or inverse lifetime) of the intermediate level.

3.1.2. Results and discussion. To compare our results with literature, the scalar, vector and tensor static dipole polarizabilities are presented in Table 5, as well as the dynamic ones for the widespread laser-trapping wavelength $\lambda = 1064$ nm (corresponding to a wave number $\sigma = 9398$ cm^{-1}). As one can notice for the ground-level scalar polarizabilities, agreement is good between the different theoretical results and which all agree well with the new measured value. The tensor static polarizability is much smaller than the scalar one in all sources; we note that our value has the same sign as the experimental one of Ref. [84]. As already pointed out in [86], we observe a strong discrepancy between our 1064-nm dynamic polarizability and the experimental value of Ref. [74]. For the $^5I_7$ level there are no literature values to our knowledge. They are actually very similar

Table 5. Real and imaginary parts of the scalar, vector and tensor dynamic dipole polarizabilities, at $\sigma = 0$ and 9398 cm^{-1} ($\lambda = 1064$ nm), for the ground $^5I_8$ and first excited level of dysprosium. Our results are compared with available literature values.

level	σ (cm^{-1})	Real part (a.u.)			Imaginary part (10^{-7} a.u.)		
		scalar	vector	tensor	scalar	vector	tensor
$^5I_8$	0	164	0	0.8	30.8	0	3.4
		165 [81], 175 [80]		-4.50 [80]			
		163 [82], 168 [83]		1.40 [84]			
	9398	193	-1.5	1.3	49.4	-11.3	5.8
		116 [74], 170 [86]					
$^5I_7$	0	163	0	0.7	30.3	0	1.7
	9398	193	-1.3	1.2	49.1	-7.9	2.9

to those of the ground level. For both levels, the main result obtained in our previous work on erbium [79] is mostly confirmed. Regarding the real part, the vector and tensor polarizability are roughly two orders of magnitudes smaller than the scalar one, which means that the trapping potential is mostly isotropic, *i.e.* they almost do not depend on the electric-field polarization or the atomic azimuthal quantum number. By contrast, the tensor, and especially vector contributions of the imaginary part represent a significant fraction of the scalar contribution, although less significant than for erbium. This makes photon-scattering anisotropic in the sense that it depends on the angle between the electric field of the trapping light and the preferential orientation of the electrons represented by the atomic azimuthal quantum number..

Figures 1 and 2 present the real, resp. imaginary, parts of the scalar, vector and tensor polarizabilities as functions of the field wavelength λ and wave number $\sigma = 1/\lambda = \omega/2\pi c$ (c being the speed of light). In order to facilitate experimental usage, we present our results in atomic units and also the corresponding relevant quantities in physical units. The real part of the polarizability is associated with the potential energy $\overline{U}$, in equivalent temperatures of microkelvins (μK), obtained for a laser intensity of 1 GW/m^2. The imaginary part is associated with the photon-scattering rate $\overline{\Gamma}$, in inverse seconds (s^{-1}), for the same intensity.

Far from atomic resonances, they confirm the two phenomena described above: (i) the strong similarity between polarizabilities of the ground and first excited levels; (ii) the isotropy of the trapping potential and anistropy of photon scattering. Moreover, for wave numbers below 10000 cm^{-1}, the polarizabilities are essentially flat, except some very narrow peaks associated with very weak transitions. On the contrary, those background values increase (in absolute value) as the wave numbers approach the strongest transitions (see Table 2).

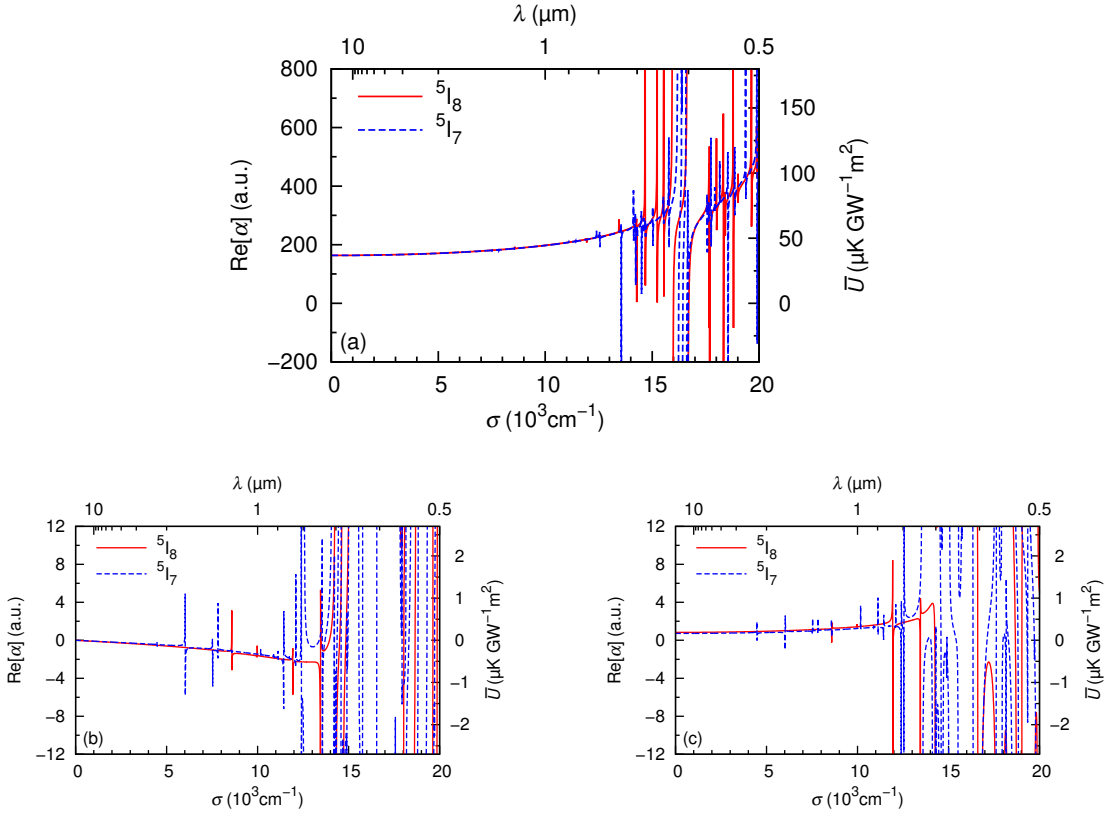

Figure 1. (Color online) Real part of the (a) scalar, (b) vector and (c) tensor dynamic dipole polarizabilities of the $^5I_8$ and $^5I_7$ levels in atomic units and corresponding trap depths obtained for an intensity of 1 GW.m^{-2}, as functions of the trapping wave number σ (or wavelength λ).

3.2. Van der Waals C_6 coefficients

Characterizing long-range interactions is crucial to understand the dynamics of ultracold gases. In the case of ground-level high-Z lanthanide atoms, the van der Waals interaction, scaling as R^{-6} (R being the interatomic distance), plays a significant role, as it competes with the magnetic-dipole interaction, scaling as R^{-3}, for distance shorter than 100 bohr. The quadrupole-quadrupole interaction is on the contrary negligible for all distances [59, 79, 97, 98]. The weak anisotropy of van der Waals interactions between lanthanide atoms is expected to be responsible for the strong density of narrow Feshbach resonances [14, 15, 97].

We consider two dysprosium atoms, A and B, in the fine-structure levels J_A and J_B of the lowest multiplet $\beta_A = \beta_B = {}^5I$ of the ground configuration $4f^{10}6s^2$. The Zeeman sublevels are characterized by the azimuthal quantum numbers M_{J_A} and M_{J_B}, taken with respect to the quantization axis z of the spaced-fixed frame. In this frame, the two atoms can perform an end-over-end rotation, characterized by the partial-wave quantum numbers L and M_L. It can be shown [99, 100] that the van der Waals interaction is represented by an effective operator $\hat{\mathrm{W}}(\mathbf{R})$, depending the vector $\mathbf{R}$ joining the two

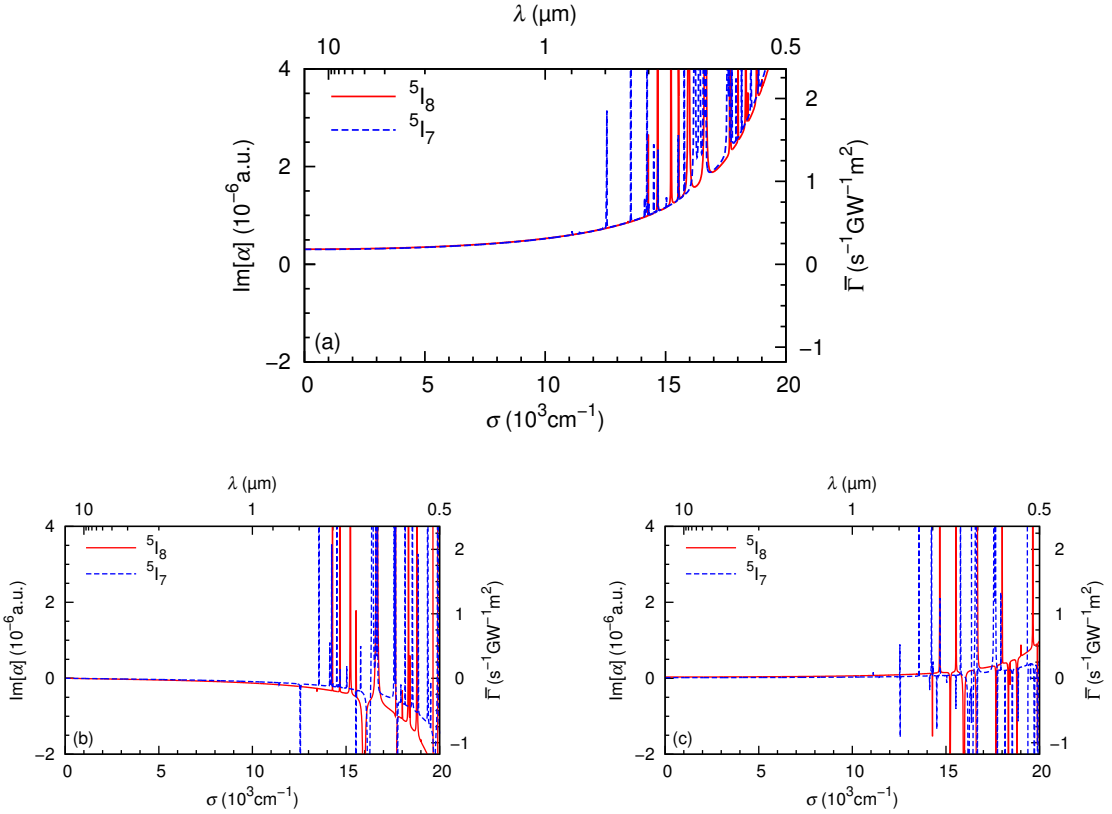

Figure 2. (Color online) Imaginary part of the (a) scalar, (b) vector and (c) tensor dynamic dipole polarizabilities of the $^5I_8$ and $^5I_7$ levels in atomic units and corresponding trap depths obtained for an intensity of 1 GW.m^{-2}, as functions of the trapping wave number σ (or wavelength λ).

atoms (from A to B). Expressed in the basis $\{|\beta_A J_A M_{J_A} \beta_B J_B M_{J_B} L M_L\rangle\}$, the matrix elements of $\hat{\mathrm{W}}(\mathbf{R})$ can be expressed as functions of a few parameters C_{6,k_Ak_B} and of angular factors,

$$\begin{aligned}
&\langle \beta_A J_A M'_{J_A} \beta_B J_B M'_{J_B} L' M'_L | \hat{\mathrm{W}}(\mathbf{R}) | \beta_A J_A M_{J_A} \beta_B J_B M_{J_B} L M_L \rangle \\
&= -\frac{C_{6,00}}{R^6} \delta_{M_{J_A} M'_{J_A}} \delta_{M_{J_B} M'_{J_B}} \delta_{LL'} \delta_{M_L M'_L} - 15 \sum_{k_A,k_B=0}^{2} (2k_A+1)(2k_B+1) \\
&\times \frac{C_{6,k_Ak_B}}{R^6} \sqrt{\frac{2L_A+1}{2L'_A+1}} \sum_{k=|k_A-k_B|}^{k_A+k_B} C^{L'0}_{L0k0} C^{k0}_{2020} \begin{Bmatrix} 1 & 1 & 2 \\ 1 & 1 & 2 \\ k_A & k_B & k \end{Bmatrix} \\
&\times \sum_{q_A=-k_A}^{k_A} \sum_{q_B=-k_B}^{k_B} \sum_{q=-k}^{k} (-1)^q C^{kq}_{k_Aq_Ak_Bq_B} C^{L'M'_L}_{LM_L,k,-q} C^{J_AM'_{J_A}}_{J_AM_{J_A}k_Aq_A} C^{J_BM'_{J_B}}_{J_BM_{J_B}k_Bq_B}
\end{aligned} \tag{10}$$

where $C^{c\gamma}_{a\alpha b\beta}$ is a Clebsch-Gordan coefficient and the number between curly brackets is a Wigner 9j-symbol [101]. The coefficients C_{6,k_Ak_B} read

$$C_{6,k_Ak_B} = \frac{2}{\sqrt{(2J_A+1)(2J_B+1)}} \sum_{\beta''_A J''_A \beta''_B J''_B} (-1)^{J_A+J''_A+J_B+J''_B} \begin{Bmatrix} 1 & 1 & k_A \\ J_A & J_A & J''_A \end{Bmatrix}$$

k_A, k_B	$^5I_8 - {}^5I_8$	$^5I_8 - {}^5I_7$	$^5I_7 - {}^5I_7$
0, 0	2273	2272	2271
1, 1	0	0	0
2, 0	-1	-1	-1
0, 2	-1	-1	-1
2, 2	0	0	0

Table 6. C_6 coefficients in atomic units, characterizing the van der Waals interactions between dysprosium atoms in the ground $^5I_8$ or first excited level $^5I_7$, as functions of the pairs of indexes k_A, k_B (see text). The case $k_A = k_B = 0$ corresponds to the so-called isotropic C_6 coefficient [99].

$$\times \left\{ \begin{array}{ccc} 1 & 1 & k_B \\ J_B & J_B & J''_B \end{array} \right\} \frac{\left| \langle \beta''_A J''_A \| \, \mathbf{d}_A \, \| \beta_A J_A \rangle \, \langle \beta''_B J''_B \| \, \mathbf{d}_B \, \| \beta_B J_B \rangle \right|^2}{E_{\beta''_A J''_A} - E_{\beta_A J_A} + E_{\beta''_B J''_B} - E_{\beta_B J_B}} \quad (11)$$

where $\{:::\}$ is a Wigner 6j-symbol [101]. In equation (10), the indexes k_A and k_B are such that $k_A + k_B$ is non-zero and even. Giving diagonal matrix elements, the coefficient $C_{6,00}$ is referred to as isotropic, while the other $C_{6,k_A k_B}$ are called anisotropic.

Table 6 displays our calculated $C_{6,k_A k_B}$ coefficients. Similarly to the case of erbium [79], the isotropic one strongly dominates the anisotropic ones. Furthermore, after diagonalization of equation (10) in the body-fixed frame, one obtains C_6 coefficients ranging from -2277 to -2271 a.u., hence 11 % larger (in absolute value) than those of Ref. [15], but with a spread roughly 30 times smaller.

4. Concluding remarks

In this article, we have characterized the optical trapping of ultracold dysprosium atoms, by calculating the real and imaginary parts of the scalar, vector and tensor contributions to the dynamic dipole polarizabilities of the ground level and the first excited level. The results indicate that the trapping potential, associated with the real part, is essentially isotropic, while the photon-scattering rate, associated with the imaginary part, exhibits a noticeable anisotropic behavior. These conclusions for the ground level are similar to our previous work on erbium, even though the anistropy of photon scattering is clearly less pronounced. The reasons for this difference are still under examination, and we expect our future work on neighboring elements (holmium and thulium) to clarify those reasons. For the 1064-nm real part of the polarizability, our results support the previous theoretical value rather than the experimental one. We also find that the polarizabilities of the ground and the first excited levels are very close, which makes them interesting candidates for optical clocks.

In order to calculate polarizabilities, we have modeled the spectrum – energy levels and transition probabilities – of neutral dysprosium. We have performed a systematic adjustment of theoretical and experimental Einstein-A coefficients. In comparison with our previous work on neutral erbium, we have incorporated in the fit transitions toward

the first excited level of dysprosium, which gives us more reliable values of the mono-electronic transition dipole moments. In addition, our detailed spectroscopic study allows us for putting into question the existence of the tabulated level $J = 9$ at 27014.02 cm^{-1}, which is however expected to have a strong transition probability towards the ground level.

Acknowledgements

The authors acknowledge support from "IFRAF/Dim Nano-K" under the project InterDy, and from "Agence Nationale de la Recherche" (ANR) under the project COPOMOL (contract ANR-13-IS04-0004-01). SN acknowledges support from European Union (ERC UQUAM) and PSL Research University (MAFAG project).

Appendix A. Energy parameters

This appendix presents the optimal parameters after the least-square fitting procedure of experimental and theoretical energies. Table A1 deals with even-parity levels, and Table A2 with odd-parity levels. The effective parameters α, β, γ with fixed values are taken for our previous work [33].

Table A1: Fitted one-configuration parameters (in cm^{-1}) for even-parity configuration of Dy I compared with HFR radial integrals. The scaling factors are $SF(P) = P_{\rm fit}/P_{\rm HFR}$, except for $E_{\rm av}$ when they are $P_{fit} - P_{HFR}$. Some parameters are constrained to vary in a constant ratio r_n, indicated in the second column except if 'fix' appears in the second or in the 'Unc.' columns. In this case, the parameter P is not adjusted. The 'Unc.' columns named after 'uncertainty' present the standard error on each parameter after the fitting procedure.

		$4f^{10}6s^2$			
Param. P	Cons.	$P_{\rm fit}$	Unc.	$P_{\rm HFR}$	SF
$E_{\rm av}$		41851	68	0	41851
$F^2(4f4f)$	r_1	83325	648	115093	0.724
$F^4(4f4f)$	r_2	56562	1128	71831	0.787
$F^6(4f4f)$	r_3	46457	689	51572	0.901
α	fix	20.0			
β	fix	-650			
γ	fix	2000			
ζ_{4f}	r_4	1770	2	1845	0.959

Table A2: Same as Table A1 but for odd-parity levels.

		$4f^9 5d6s^2$				$4f^{10} 6s6p$			
Param. P	Cons.	$P_{\rm fit}$	Unc.	$P_{\rm HFR}$	SF	$P_{\rm fit}$	Unc.	$P_{\rm HFR}$	SF
$E_{\rm av}$		68280	97	5400	62880	61716	66	14794	46922
$F^2(4f4f)$	r_1	91462	471	122573	0.746	85931	443	115161	0.746
$F^4(4f4f)$	r_2	61462	739	76869	0.800	57486	691	71875	0.800
$F^6(4f4f)$	r_3	48518	462	55292	0.877	45282	431	51604	0.877
α	fix	20.0				20.0			
β	fix	-650				-650			
γ	fix	2000				2000			
ζ_{4f}	r_4	1901	3	1975	0.963	1777	3	1846	0.963
ζ_{5d}	r_{10}	727	12	890	0.817				
ζ_{6p}	r_6					1372	12	947	1.449
$F^1(4f5d)$	r_{11}	658	99						
$F^2(4f5d)$	r_{12}	15708	132	20992	0.748				
$F^4(4f5d)$	r_{13}	11704	223	9652	1.213				
$F^1(4f6p)$	r_7					112	38		
$F^2(4f6p)$	r_8					3093	268	3386	0.913
$G^1(4f5d)$	r_{14}	5785	110	9181	0.630				
$G^2(4f5d)$	r_{15}	2071	255						
$G^3(4f5d)$	r_{16}	6731	288	7278	0.925				
$G^4(4f5d)$	r_{17}	4003	393						
$G^5(4f5d)$	r_{18}	5480	236	5501	0.996				
$G^3(4f6s)$	r_9					1132	51	1688	0.670
$G^2(4f6p)$	r_5					1032	17	774	1.333
$G^4(4f6p)$	r_5					900	15	675	1.333
$G^1(6s6p)$	fix					10292		23189	0.444
configuration-interaction		$4f^9 5d6s^2 - 4f^{10} 6s6p$							
$R^1(5d6s, 4f6p)$	r_5	-3545	58	-4648	0.763				
$R^3(5d6s, 6p4f)$	r_5	-748	12	-980	0.763				

Bibliography

[1] M.A. Baranov. Theoretical progress in many-body physics with ultracold dipolar gases. *Phys. Rep.*, 464(3):71–111, 2008.

[2] T. Lahaye, C. Menotti, L. Santos, M. Lewenstein, and T. Pfau. The physics of dipolar bosonic quantum gases. *Rep. Prog. Phys.*, 72(12):126401, 2009.

[3] F. Dalfovo, S. Giorgini, L. P. Pitaevskiĭ, and S. Stringari. Theory of Bose-Einstein condensation in trapped gases. *Rev. Mod. Phys.*, 71(3):463–512, 1999.

[4] W. Zhang, D.F. Walls, and B.C. Sanders. Atomic soliton in a traveling wave laser beam. *Phys. Rev. Lett.*, 72:60–63, 1994.

[5] W. Zhang and D.F. Walls. Quantum field theory of interaction of ultracold atoms with a light wave: Bragg scattering in nonlinear atom optics. *Phys. Rev. A*, 49:3799–3813, 1994.

[6] K. Góral, K. Rzążewski, and T. Pfau. Bose-Einstein condensation with magnetic dipole-dipole forces. *Phys. Rev. A*, 61:051601, 2000.

[7] H. Pu, W. Zhang, and P. Meystre. Ferromagnetism in a lattice of bose-einstein condensates. *Phys. Rev. Lett.*, 87:140405, 2001.

[8] J. Stuhler, A. Griesmaier, T. Koch, M. Fattori, T. Pfau, S. Giovanazzi, P. Pedri, and L. Santos. Observation of dipole-dipole interaction in a degenerate quantum gas. *Phys. Rev. Lett.*, 95:150406, 2005.

[9] T. Lahaye, T. Koch, B. Fröhlich, M. Fattori, J. Metz, A. Griesmaier, S. Giovanazzi, and T. Pfau. Strong dipolar effects in a quantum ferrofluid. *Nature*, 448(7154):672–675, 2007.

[10] G. Bismut, B. Laburthe-Tolra, E. Maréchal, P. Pedri, O. Gorceix, and L. Vernac. Anisotropic excitation spectrum of a dipolar quantum bose gas. *Phys. Rev. Lett*, 109:155302, 2012.

[11] A. de Paz, A. Sharma, A. Chotia, E. Maréchal, J.H. Huckans, P. Pedri, L. Santos, O. Gorceix, L. Vernac, and B. Laburthe-Tolra. Nonequilibrium quantum magnetism in a dipolar lattice gas. *Phys. Rev. Lett.*, 111:185305, 2013.

[12] K. Baumann, N.Q. Burdick, M. Lu, and B.L. Lev. Observation of low-field Fano-Feshbach resonances in ultracold gases of dysprosium. *Phys. Rev. A*, 89:020701, 2014.

[13] K. Aikawa, S. Baier, A. Frisch, M. Mark, C. Ravensbergen, and F. Ferlaino. Observation of Fermi surface deformation in a dipolar quantum gas. *Science*, 345(6203):1484–1487, 2014.

[14] A. Frisch, M. Mark, K. Aikawa, F. Ferlaino, J.L. Bohn, C. Makrides, A. Petrov, and S. Kotochigova. Quantum chaos in ultracold collisions of gas-phase erbium atoms. *Nature*, 507(7493):475–479, 2014.

[15] T. Maier, H. Kadau, M. Schmitt, M. Wenzel, I. Ferrier-Barbut, T. Pfau, A. Frisch, S. Baier, K. Aikawa, L. Chomaz, M.J. Mark, F. Ferlaino, C. Makrides, E. Tiesinga, A. Petrov, and S. Kotochigova. Emergence of chaotic scattering in ultracold Er and Dy. *Phys. Rev. X*, 5:041029, 2015.

[16] M.D. Lukin, M. Fleischhauer, R. Cöté, L.M. Duan, D. Jaksch, J.I. Cirac, and P. Zoller. Dipole blockade and quantum information processing in mesoscopic atomic ensembles. *Phys. Rev. Lett.*, 87:037901, 2001.

[17] A. Micheli, G.K. Brennen, and P. Zoller. A toolbox for lattice-spin models with polar molecules. *Nature Phys.*, 2(5):341–347, 2006.

[18] I. Bloch, J. Dalibard, and S. Nascimbène. Quantum simulations with ultracold quantum gases. *Nature Phys.*, 8(4):267–276, 2012.

[19] V. Galitski and I. B. Spielman. Spin-orbit coupling in quantum gases. *Nature*, 494(7435):49–54, 2013.

[20] T.F. Gallagher. *Rydberg Atoms*. Cambridge University Press, 1994.

[21] W.R. Anderson, J.R. Veale, and T.F. Gallagher. Resonant dipole-dipole energy transfer in a nearly frozen Rydberg gas. *Phys. Rev. Lett.*, 80(2):249–252, 1998.

[22] K. Afrousheh, P. Bohlouli-Zanjani, D. Vagale, A. Mugford, M. Fedorov, and J.D.D. Martin. Spectroscopic observation of resonant electric dipole-dipole interactions between cold Rydberg atoms. *Phys. Rev. Lett*, 93:233001, 2004.

[23] W. Li, P.J. Tanner, and T.F. Gallagher. Dipole-dipole excitation and ionization in an ultracold gas of Rydberg atoms. *Phys. Rev. Lett.*, 94:173001, 2005.

[24] T. Vogt, M. Viteau, J. Zhao, A. Chotia, D. Comparat, and P. Pillet. Dipole blockade at förster resonances in high resolution laser excitation of Rydberg states of cesium atoms. *Phys. Rev. Lett.*, 97:083003, 2006.

[25] E. Brion, K. Mølmer, and M. Saffman. Quantum computing with collective ensembles of multilevel systems. *Physical review letters*, 99:260501, 2007.

[26] C.S.E. Van Ditzhuijzen, A.F. Koenderink, J.V. Hernández, F. Robicheaux, L.D. Noordam, and H.B. Van Linden Van Den Heuvell. Spatially resolved observation of dipole-dipole interaction between Rydberg atoms. *Phys. Rev. Lett.*, 100:243201, 2008.

[27] A. Gaëtan, Y. Miroshnychenko, T. Wilk, A. Chotia, M. Viteau, D. Comparat, P. Pillet,

A. Browaeys, and P. Grangier. Observation of collective excitation of two individual atoms in the Rydberg blockade regime. *Nature Physics*, 5(2):115–118, 2009.

[28] M. Saffman, T.G. Walker, and K. Mølmer. Quantum information with Rydberg atoms. *Rev. Mod. Phys.*, 82(3):2313–2363, 2010.

[29] N. Thaicharoen, L.F. Gonçalves, and G. Raithel. Atom-pair kinetics with strong electric-dipole interactions. *Phys. Rev. Lett.*, 116:213002, 2016.

[30] A. Micheli, G. Pupillo, H. P. Büchler, and P. Zoller. Cold polar molecules in two-dimensional traps: Tailoring interactions with external fields for novel quantum phases. *Phys. Rev. A*, 76:043604, 2007.

[31] J.N. Byrd, J.A. Montgomery Jr, and R. Côté. Long-range forces between polar alkali-metal diatoms aligned by external electric fields. *Phys. Rev. A*, 86:032711, 2012.

[32] P.S. Żuchowski, M. Kosicki, M. Kodrycka, and P. Soldán. van der Waals coefficients for systems with ultracold polar alkali-metal molecules. *Phys. Rev. A*, 87(2):022706, 2013.

[33] M. Lepers, R. Vexiau, M. Aymar, N. Bouloufa-Maafa, and O. Dulieu. Long-range interactions between polar alkali-metal diatoms in external electric fields. *Phys. Rev. A*, 88:032709, 2013.

[34] R. Vexiau, M. Lepers, M. Aymar, N. Bouloufa-Maafa, and O. Dulieu. Long-range interactions between polar bialkali ground-state molecules in arbitrary vibrational levels. *J. Chem. Phys.*, 142:214303, 2015.

[35] J. Deiglmayr, M. Aymar, R. Wester, M. Weidemüller, and O. Dulieu. Calculations of static dipole polarizabilities of alkali dimers: Prospects for alignment of ultracold molecules. *J. Chem. Phys.*, 129:064309, 2008.

[36] K.-K. Ni, S. Ospelkaus, M. H. G. de Miranda, A. Peer, B. Neyenhuis, J. J. Zirbel, S. Kotochigova, P. S. Julienne, D. S. Jin, and J. Ye. A high phase-space-density gas of polar molecules. *Science*, 322(5899):231–235, 2008.

[37] S. Ospelkaus, K-K Ni, G. Quéméner, B. Neyenhuis, D. Wang, M.H.G. deMiranda, J.L. Bohn, J. Ye, and D.S. Jin. Controlling the hyperfine state of rovibronic ground-state polar molecules. *Phys. Rev. Lett.*, 104(3):030402, 2010.

[38] K. Aikawa, D. Akamatsu, M. Hayashi, K. Oasa, J. Kobayashi, P. Naidon, T. Kishimoto, M. Ueda, and S. Inouye. Coherent transfer of photoassociated molecules into the rovibrational ground state. *Phys. Rev. Lett.*, 105(20):203001, 2010.

[39] T. Takekoshi, L. Reichsöllner, A. Schindewolf, J.M. Hutson, C.R. Le Sueur, O. Dulieu, F. Ferlaino, R. Grimm, and H.-C. Nägerl. Ultracold dense samples of dipolar RbCs molecules in the rovibrational and hyperfine ground state. *Phys. Rev. Lett.*, 113:205301, 2014.

[40] P. K. Molony, P. D. Gregory, Z. Ji, B. Lu, M. P. K´oppinger, C. R. Le Sueur, C. L. Blackley, J. M. Hutson, and S. L. Cornish. Creation of ultracold $^{87}Rb^{133}Cs$ moleculaes in the rovibrational ground state. *Phys. Rev. Lett.*, 113(25):255301, 2014.

[41] J.W. Park, S.A. Will, and M.W. Zwierlein. Ultracold dipolar gas of fermionic $^{23}Na^{40}K$ molecules in their absolute ground state. *Phys. Rev. Lett.*, 114:205302, 2015.

[42] B. Zhu, X.K. Li, X.D. He, M.Y. Guo, F.D. Wang, R. Vexiau, N. Bouloufa-Maafa, O. Dulieu, and D.J. Wang. Long-range states of the narb molecule near the Na($3^2S_1/2$)+ Rb($5^2P_3/2$) asymptote. *Phys. Rev. A*, 93:012508, 2016.

[43] B. K. Stuhl, M. T. Hummon, M. Yeo, G. Quéméner, J. L. Bohn, and J. Ye. Evaporative cooling of the dipolar hydroxyl radical. *Nature*, 492:396–400, 2012.

[44] J. F. Barry, D. J. McCarron, E. B. Norrgard, M. H. Steinecker, and D. Demille. *Nature*, 512:286, 2014.

[45] M. Yeo, M. T Hummon, A. L. Collopy, B. Yan, B. Hemmerling, E. Chae, J. M. Doyle, and J. Ye. Rotational state microwave mixing for laser cooling of complex diatomic molecules. *Phys. Rev. Lett.*, 114(22):223003, 2015.

[46] B. Pasquiou, A. Bayerle, S. M. Tzanova, S. Stellmer, J.Szczepkowski, M. Parigger, R. Grimm, and F. Schreck. Quantum degenerate mixtures of strontium and rubidium atoms. *Phys. Rev. A*, 88(2):023601, 2013.

[47] A. Griesmaier, J. Werner, S. Hensler, J. Stuhler, and T. Pfau. Bose-Einstein condensation of chromium. *Phys. Rev. Lett.*, 94(16):160401, 2005.

[48] B. Naylor, A. Reigue, E. Maréchal, O. Gorceix, B. Laburthe-Tolra, and L. Vernac. Chromium dipolar fermi sea. *Phys. Rev. A*, 91:011603, 2015.

[49] C.I. Hancox, S.C. Doret, M.T. Hummon, L. Luo, and J.M. Doyle. Magnetic trapping of rare-earth atoms at millikelvin temperatures. *Nature*, 431(7006):281–284, 2004.

[50] B. Hemmerling, G.K. Drayna, E. Chae, A. Ravi, and J.M. Doyle. Buffer gas loaded magneto-optical traps for Yb, Tm, Er and Ho. *New J. Phys.*, 16:063070, 2014.

[51] N. Leefer, A. Cingöz, B. Gerber-Siff, A. Sharma, J.R. Torgerson, and D. Budker. Transverse laser cooling of a thermal atomic beam of dysprosium. *Phys. Rev. A*, 81:043427, 2010.

[52] M. Lu, S.H. Youn, and B.L. Lev. Trapping ultracold dysprosium: A highly magnetic gas for dipolar physics. *Phys. Rev. Lett.*, 104(6):063001, 2010.

[53] T. Maier, H. Kadau, M. Schmitt, A. Griesmaier, and T. Pfau. Narrow-line magneto-optical trap for dysprosium atoms. *Opt. Lett.*, 39(11):3138–3141, 2014.

[54] H. Ban, M. Jacka, J. Hanssen, J. Reader, and J. McClelland. Laser cooling transitions in atomic erbium. *Opt. Express*, 13(8):3185–3195, 2005.

[55] J.J. McClelland and J.L. Hanssen. Laser cooling without repumping: A magneto-optical trap for erbium atoms. *Phys. Rev. Lett.*, 96(14):143005, 2006.

[56] A. Frisch, K. Aikawa, M. Mark, A. Rietzler, J. Schindler, E. Zupanič, R. Grimm, and F. Ferlaino. Narrow-line magneto-optical trap for erbium. *Phys. Rev. A*, 85(5):051401, 2012.

[57] J. Miao, J. Hostetter, G. Stratis, and M. Saffman. Magneto-optical trapping of holmium atoms. *Phys. Rev. A*, 89:041401, 2014.

[58] D. Sukachev, A. Sokolov, K. Chebakov, A. Akimov, S. Kanorsky, N. Kolachevsky, and V. Sorokin. Magneto-optical trap for thulium atoms. *Phys. Rev. A*, 82(1):011405, 2010.

[59] A. Frisch, M. Mark, K. Aikawa, S. Baier, R. Grimm, A. Petrov, S. Kotochigova, G. Quéméner, M. Lepers, O. Dulieu, and F. Ferlaino. Ultracold polar molecules composed of strongly magnetic atoms. *Phys. Rev. Lett.*, 115(20):203201, 2015.

[60] X. Cui, B. Lian, T.-L. Ho, B.L. Lev, and H. Zhai. Synthetic gauge field with highly magnetic lanthanide atoms. *Phys. Rev. A*, 88:011601, 2013.

[61] N.Q. Burdick, Y. Tang, and B.L. Lev. A long-lived spin-orbit-coupled degenerate dipolar fermi gas. *arXiv preprint arXiv:1605.03211*, 2016.

[62] L. Brewer. *Systematics of the Properties of the Lanthanides*. Ed. S.P. Sinha, D Reidel Publ. Co, 1983.

[63] A. Kramida, Yu. Ralchenko, J. Reader, and and NIST ASD Team. NIST Atomic Spectra Database (ver. 5.3), [Online]. Available: `http://physics.nist.gov/asd` [2016, March 8]. National Institute of Standards and Technology, Gaithersburg, MD., 2015.

[64] G. Nave and U. Griesmann. New energy levels and classifications of spectral lines from neutral and singly-ionized dysprosium (Dy I and Dy II). *Phys. Scr.*, 62(6):463–473, 2000.

[65] J.-F. Wyart. An interpretation of Dy I and Ho I energy levels in the ground state parity. in preparation.

[66] D. Budker, D. DeMille, E. D. Commins, and M. S. Zolotorev. Investigation of nearly degenerate opposite parity states in atomic dysprosium. *Phys. Rev. Lett.*, 70(20):3019, 1993.

[67] D. Budker, D. DeMille, E.D. Commins, and M.S. Zolotorev. Experimental investigation of excited states in atomic dysprosium. *Phys. Rev. A*, 50(1):132–143, 1994.

[68] A Cingöz, A Lapierre, A-T Nguyen, N Leefer, D Budker, S K Lamoreaux, and J R Torgerson. Limit on the temporal variation of the fine-structure constant using atomic dysprosium. *Phys. Rev. Lett.*, 98(4):040801, 2007.

[69] N Leefer, CTM Weber, A Cingöz, JR Torgerson, and D Budker. New limits on variation of the fine-structure constant using atomic dysprosium. *Phys. Rev. Lett.*, 111(6):060801, 2013.

[70] A. Kozlov, V.A. Dzuba, and V.V. Flambaum. Prospects of building optical atomic clocks using Er I or Er III. *Phys. Rev. A*, 88(3):032509, 2013.

[71] D. Sukachev, S. Fedorov, I. Tolstikhina, G. Kalganova, E .and Vishnyakova, K. Khabarova, D. Tregubov, A. Golovizin, V. Sorokin, and N. Kolachevsky. Inner-shell magnetic dipole transition in tm atom as a candidate for optical lattice clocks. *Phys. Rev. A*, 94:022512, 2016.

[72] K. Aikawa, A. Frisch, M. Mark, S. Baier, A. Rietzler, R. Grimm, and F. Ferlaino. Bose-Einstein condensation of erbium. *Phys. Rev. Lett.*, 108(21):210401, 2012.

[73] K. Aikawa, A. Frisch, M. Mark, S. Baier, R. Grimm, and F. Ferlaino. Reaching Fermi degeneracy via universal dipolar scattering. *Phys. Rev. Lett.*, 112:010404, 2014.

[74] M. Lu, N.Q. Burdick, S.H. Youn, and B.L. Lev. Strongly dipolar Bose-Einstein condensate of dysprosium. *Phys. Rev. Lett.*, 107(19):190401, 2011.

[75] M. Lu, N.Q. Burdick, and B.L. Lev. Quantum degenerate dipolar Fermi gas. *Phys. Rev. Lett.*, 108:215301, 2012.

[76] Y. Tang, N.Q. Burdick, K. Baumann, and B.L. Lev. Bose-Einstein condensation of ^{162}Dy and ^{160} Dy. *New J. Phys.*, 17:045006, 2015.

[77] R. Grimm, M. Weidemüller, and Y.B. Ovchinnikov. Optical dipole traps for neutral atoms. *Adv. At. Mol. Opt. Phys.*, 42:95–170, 2000.

[78] N.L. Manakov, V.D. Ovsiannikov, and L.P. Rapoport. Atoms in a laser field. *Phys. Rep.*, 141(6):320–433, 1986.

[79] M. Lepers, J.-F. Wyart, and O. Dulieu. Anisotropic optical trapping of ultracold erbium atoms. *Phys. Rev. A*, 89:022505, 2014.

[80] Xi Chu, A. Dalgarno, and G.C. Groenenboom. Dynamic polarizabilities of rare-earth-metal atoms and dispersion coefficients for their interaction with helium atoms. *Phys. Rev. A*, 75(3):032723, 2007.

[81] D.R. Lide. *CRC handbook of chemistry and physics*. CRC press, 2012.

[82] V.A. Dzuba, A. Kozlov, and V.V. Flambaum. Scalar static polarizabilities of lanthanides and actinides. *Phys. Rev. A*, 89(4):042507, 2014.

[83] VA Dzuba. Ionization potentials and polarizabilities of superheavy elements from db to cn (z= 105 to 112). *arXiv preprint arXiv:1602.08190*, 2016.

[84] R.-H. Rinkleff and F. Thorn. On the tensor polarizabilities in the $4f^N6s2$ ground levels of the neutral rare-earth atoms. *Z. Phys. D*, 32(3):173–177, 1994.

[85] L. Ma, J. Indergaard, B. Q. Zhang, I. Larkin, R. Moro, and W. A. de Heer. Measured atomic ground-state polarizabilities of 35 metallic elements. *Phys. Rev. A*, 91:010501R, 2015.

[86] V.A. Dzuba, V.V. Flambaum, and B.L Lev. Dynamic polarizabilities and magic wavelengths for dysprosium. *Phys. Rev. A*, 83(3):032502, 2011.

[87] R. D. Cowan. The theory of atomic structure and spectra. 3, 1981.

[88] J.-F. Wyart. On the interpretation of complex atomic spectra by means of the parametric Racah–Slater method and Cowan codes. *Can. J. Phys.*, 89(4):451–456, 2011.

[89] M. Lepers, Y. Hong, J.-F. Wyart, and O. Dulieu. Proposal for laser cooling of rare-earth ions. *Phys. Rev. A*, 93:011401R, 2016.

[90] J.-F. Wyart and J.E. Lawler. Theoretical interpretation and new energy levels in Er II. *Phys. Scr.*, 79(4):045301, 2009.

[91] J. Ruczkowski, M. Elantkowska, and J. Dembczyński. An alternative method for determination of oscillator strengths: The example of Sc II. *J. Quant. Spectr. Radiat. Transfer*, 145:20–42, 2014.

[92] S. Bouazza, P. Quinet, and P. Palmeri. Semi-empirical studies of atomic transition probabilities, oscillator strengths and radiative lifetimes in Hf II. *J. Quant. Spectr. Radiat. Transfer*, 163:39–49, 2015.

[93] W.C. Martin, R. Zalubas, and L. Hagan. Atomic energy levels–the rare-earth elements. *Stand. Ref. Data Ser. (National Bureau of Standards, US)*, 60:332–338, 1978.

[94] A. Kramida. *PC version of the Cowan codes*. Avaliable at http://das101.isan.troitsk.ru/COWAN, 2010.

[95] J.-F. Wyart. Interpretation du spectre de Dy I: I. etude des configurations impaires. *Physica*, 75(2):371–385, 1974.

[96] ME Wickliffe, JE Lawler, and G Nave. Atomic transition probabilities for dy i and dy ii. *J. Quant. Spectrosc. Ra.*, 66(4):363–404, 2000.

[97] S. Kotochigova and A. Petrov. Anisotropy in the interaction of ultracold dysprosium. *Phys. Chem. Chem. Phys.*, 13(42):19165–19170, 2011.

[98] M. Lepers, G. Quéméner, E. Luc-Koenig, and O. Dulieu. Four-body long-range interactions between ultracold weakly-bound diatomic molecules. *J. Phys. B.*, 49:014004, 2016.

[99] A.J. Stone. *The Theory of Intermolecular Forces*. Oxford University Press, New York, 1996.

[100] I.G. Kaplan. *Intermolecular interactions: physical picture, computational methods and model potentials*. John Wiley & Sons, 2006.

[101] D.A. Varshalovich, A.N. Moskalev, and V.K. Khersonskii. *Quantum theory of angular momentum*. World Scientific, 1988.